Journal of Food and Drug Analysis

Volume 32 | Issue 3 Article 8

Optimization, physicochemical stability and in vivo study of alginate-chitosan composites as nanocarriers for low molecular weight angiotensin I-converting enzyme (ACE)-inhibitory peptide

ORIGINAL ARTICLE

Optimization, physicochemical stability and *in vivo* study of alginate-chitosan composites as nanocarriers for low molecular weight angiotensin I-converting enzyme (ACE)-inhibitory peptide

Shehu Muhammad Auwal [a,b], Siti Balqis Muhammad Ghanisma [a], Nazamid Saari [a,*]

[a] Department of Food Science, Faculty of Food Science and Technology, Universiti Putra Malaysia, UPM, 43400, Serdang, Selangor, Malaysia
[b] Department of Biochemistry, Faculty of Basic Medical Sciences, Bayero University, Kano 700231, Nigeria

Abstract

Chitosan and alginate, are non-toxic and biodegradable polymers used to enhance the stability of biotherapeutics by loading them into nanocarriers. In this study, the stone fish-derived low molecular weight peptide (Ala-Leu-Gly-Pro-Gln-Phe-Tyr), exhibited an *in vitro* ACE-inhibitory activity of 94.43 ± 2.05% and an IC_{50} of 0.012 ± 0.001 mM. The peptide was encapsulated via ionic gelation with alginate followed by polyelectrolyte complexation with chitosan. The resulting ACE-inhibitory peptide-loaded alginate-chitosan nanoparticles (ACE-I-ALG-CS NPs) were optimized to achieve small particle size (212.60 nm) and high encapsulation efficiency (EE, 74.48%). This was based on an optimum chitosan concentration (0.420%w/v), homogenization speed (6000 rpm), and homogenization time (30 min) using Box Behnken experimental design (BBED). Characterization of the ACE-I-ALG-CS NPs revealed a spherical, monodispersed morphology with high physicochemical stability during storage at 2 °C, 7 °C, and 12 °C for 12 weeks. Moreover, the *in vivo* study conducted on spontaneously hypertensive rats (SHRs) demonstrated a significantly higher ($p < 0.05$) systolic blood pressure (SBP)-lowering effect of the ACE-I-ALG-CS NPs compared to captopril and unencapsulated peptide. Hence, alginate and chitosan can be used as biocompatible coating materials to enhance the stability and *in vivo* antihypertensive effect of Ala-Leu-Gly-Pro-Gln-Phe-Tyr through encapsulation, thereby making it potentially valuable for various applications in pharmaceuticals and food industry.

Keywords: Antihypertensive, Biotherapeutics, Nanocarriers, Optimization, Peptide

1. Introduction

Biologically active peptides derived from various food sources have been identified as safe oral ACE-inhibitors, effectively modulating blood pressure by reducing angiotensin II synthesis and increasing bradykinin formation [1–3]. However, maintaining the structural and functional integrity of these peptides poses challenges, including stability during storage and resistance to gastrointestinal conditions following oral administration [4–6].

To address these challenges, various strategies such as structural modification, permeation enhancers, and encapsulation using carrier particles have been employed to enhance the stability, bioavailability, and functionality of biotherapeutic peptides [7–9]. Among these approaches, encapsulation using nanocarriers is particularly promising, improving stability, solubility, and sensory properties of peptides [4,10,11]. Specifically, nanocarriers fabricated with alginate and chitosan have shown potential due to their safety and biodegradability [12–14]. Alginate and chitosan or their composites have been used as edible coatings to enhance the shelf life, for long term preservation of susceptible materials [15,16].

However, challenges arise when using alginate and chitosan individually due to their pH sensitivity and

Received 10 March 2024; accepted 10 July 2024.
Available online 13 September 2024

* Corresponding author.
E-mail address: nazamid@upm.edu.my (N. Saari).

https://doi.org/10.38212/2224-6614.3522

insufficient barrier properties [17]. Complexation of these polymers can overcome these limitations, improving their pH sensitivity, mucoadhesiveness and release properties [7,13,18]. This blend will overcome the individual limitations by creating stable nanocomposites with enhanced stability against physicochemical degradation [19,20].

Optimization of the alginate-chitosan blend is crucial for effective nanocarrier fabrication, with favorable strategies like Box-Behnken experimental design [20,21]. This approach enables identification of optimal parameters for smaller particle size and higher EE, enhancing physicochemical stability and *in vivo* efficacy [20,22]. Previous studies have highlighted the potential of specific peptides such as Ala-Leu-Gly-Pro-Gln-Phe-Tyr derived from stone fish, for ACE-inhibitory activity and other bioactive properties [1,4]. The stone fish is an underutilized specie of sea cucumber with many nutritional and health benefits. It is commonly found in Malaysia and other countries along the coastal areas. However, the *in vivo* efficacy of the peptides may be limited by gastrointestinal barriers, necessitating their stabilization for enhanced delivery and efficacy [20]. Therefore, the use of alginate and chitosan in the preparation of nanocarriers to encapsulate the peptide, is to synergistically enhance its stability, oral-colon delivery, controlled release, absorption, bioavailability and *in vivo* antihypertensive efficacy higher than by the individual polymers [13].

Hence, the present study was aimed to stabilize the Ala-Leu-Gly-Pro-Gln-Phe-Tyr by loading it into alginate-chitosan nanocarriers, optimized using Box-Behnken design. The optimized nanocarriers are biodegradable and can effectively preserve the peptide for safe delivery via oral route. Thus, making the polymers an ideal choice for specific food and biomedical applications [23]. Therefore, the current approach seeks to enhance the physicochemical stability and systolic blood pressure lowering efficacy of the optimized peptide-loaded nanocarriers in SHRs.

2. Materials and methods

2.1. Materials

Low molecular weight chitosan powder (85% degree of deacetylation), medium viscosity sodium alginate, sodium tripolyphosphate (85% purity), N-hippuryl-Histidyl-Leucine tetrahydtare (HHL), ACE derived from rabbit lung, and Bichinchoninic acid (BCA) micro protein assay kit were provided by Sigma-Aldrich, Co. (Spruce St., St. Louis, MO, USA). Tween 80 was purchased from Merck Schuchardt OHG (Hohenbrunn, Germany), while the Ala-Leu-Gly-Pro-Gln-Phe-Tyr (low molecular weight) was produced by GenScript Biotech (New Jersey, USA). Mono and dibasic potassium salts were obtained from Merck KGaA (Darmstadt, Germany). All other chemicals and reagents used were of analytical grades and purchased from Merck KGaA (Darmstadt, Germany), Fisher Scientific (Loughborough, Leics, UK), and Sigma-Aldrich, Co. (St. Louis, MO, USA), unless otherwise specified.

Male SHRs, aged 15 weeks and weighing between 250 and 320 g, were procured from the service unit of animal experiments, Universiti Malaya, Malaysia. Ethical permission to utilize rats was granted by the Universiti Putra Malaysia committee for animal care and use, under the AUP Number R078_2015.

2.2. Determination of in vitro ACE-inhibitory effect and IC_{50}

The Ala-Leu-Gly-Pro-Gln-Phe-Tyr was obtained through solid phase synthesis for peptides with $\geq$5 amino acids (percentage purity >90%) by Genscript (New Jersey, USA). The ACE-inhibitory activity was assayed according to the method described by Jimsheena and Gowda [24] as modified by Auwal et al. [1]. In the assay, 15 μL of the peptide was incubated with 10 μL of 100 mU/mL ACE at 37 °C for 10 min. Subsequently, 50 μL of 5 mM HHL (prepared in 300 mM NaCl and 50 mM borate buffer pH 8.3) was added, and the incubation continued for 60 min. The reaction was then stopped by adding a 1 M solution of HCl, followed by the addition of 150 μL of pyridine and 75 μL of benzene sulfonyl chloride (BSC). The released hippuric acid was quantified based on the intensity of the yellow color produced using a microplate reader at 410 nm. The inhibitory effect of the peptide against ACE was determined as an average of three observations according to the relation as follow:

$$\text{ACE} - \text{inhibition}\,(\%) = \frac{(\text{Ac} - \text{As})}{(\text{Ac} - \text{Ab})} \times 100 \qquad (1)$$

Where:

Ac: Absorbance value of control containing ACE and HHL; As: Absorbance value of sample containing peptide, ACE and HHL, Ab: Absorbance of blank containing only HHL.

The IC_{50}, which refers to the concentration of a peptide needed to exhibit 50% of ACE-inhibitory effect was calculated from a non-linear regression plot of ACE inhibitory effect versus peptide concentration using GraphPad Prism 7 software (GraphPad Software Inc., California, USA).

2.3. Preparation of the ACE-I-ALG-CS NPs

Chitosan and alginate solutions were prepared at a concentration of 5 mg/mL in 1% acetic acid and distilled water, respectively. Similarly, sodium tripolyphosphate and calcium chloride were prepared at 5 mg/mL, and Tween 80 at 0.5% (v/v). To produce the ACE-I-ALG-CS NPs, the peptide solution was mixed with surfactant at 1:4 Peptide:Tween 80 volume ratio. The mixture was gently added to the alginate solution at 1:1 Alginate:Tween 80 volume ratio while homogenizing for 5 min. A solution of $CaCl_2$ was then added to the mixture at 1:1 $CaCl_2$:Tween 80 volume ratio, followed by the addition of chitosan at 2:1 Chitosan:Alginate volume ratio and TPP at 4:1 Chitosan:TPP volume ratio, respectively. The process continued until an opalescent suspension of ACE-I-ALG-CS NPs appeared. The suspension was then centrifuged at 10,000×g for 10 min, and the pellet was resuspended in phosphate buffer and ice-bath sonicated at 40 Hz for 10 min before further analysis.

2.4. Characterization of the ACE-I-ALG-CS NPs

The physicochemical properties of ACE-I-ALG-CS NPs, including particle size, polydispersity index (pdi), and zeta potential (ζ), were assessed using dynamic light scattering (DLS). Additionally, the morphology of the NPs was examined while the EE and changes in physicochemical properties during the 12-weeks of storage were determined.

2.4.1. Dynamic light scattering and surface morphology of ACE-I-ALG-CS NPs

A Zetasizer Nano ZSP (Malvern Panalytical Ltd., Malvern, UK) was used to measure particle size, pdi, and ζ. The stability of the NPs was monitored by observing changes in these parameters over time. The surface morphology was evaluated using TEM (JEM-2100F, JEOL Ltd., Tokyo, Japan).

2.4.2. Determination of encapsulation efficiency of ACE-I-ALG-CS NPs

The EE of the ACE-I-ALG-CS NPs was calculated by subtracting the amount of residual peptide in the supernatant after centrifugation from the total amount of peptide initially added for encapsulation according to the following relation:

$$EE(\%) = \frac{\text{Total amount of peptide} - \text{residual amount of peptide}}{\text{Total amount of peptide}} \times 100 \quad (2)$$

2.5. Physicochemical storage stability study of ACE-I-ALG-CS NPs

The physicochemical storage stability of ACE-I-ALG-CS NPs was investigated by storing the NPs at different temperatures (2 °C, 7 °C, and 12 °C) for 12 weeks. Changes in particle size, pdi, ζ and EE were assessed weekly for 12 weeks.

2.6. Experimental design and model building for the optimization of ACE-I-ALG-CS NPs

Experimental design and model building for optimization of ACE-I-ALG-CS NPs were conducted using Minitab v. 16 software (Minitab, State College, PA). The Box-Behnken method, based on response surface methodology (RSM) was used to analyze the effects of input variables (chitosan concentration, homogenization speed, and homogenization time) on output variables (particle size and EE) (Table 1). The second-order polynomial function was used to model the relationship between input variables and responses, allowing for assessment of linear, interaction, and quadratic effects.

The formula is as follows:

$$Y = \beta_0 + \beta_1\chi_1 + \beta_2\chi_2 + \beta_3\chi_3 + \beta_{11}\chi_1^2 + \beta_{22}\chi_2^2 + \beta_{33}\chi_3^2 + \beta_{12}\chi_1\chi_2 + \beta_{13}\chi_1\chi_3 + \beta_{23}\chi_2\chi_3 \quad (3)$$

Where Y represents the predicted response, β_0 is the intercept, β_1, β_2, and β_3 denote linear coefficients, β_{11}, β_{22}, and β_{33} represent squared coefficients, and β_{12}, β_{13}, and β_{23} stand for interaction coefficients. The values χ_1, χ_2, and χ_3 correspond to the input variables.

Analysis of variance (ANOVA) was performed to determine the effect of the input variables on the response at a significance of $p < 0.05$. The fitness of the second order polynomial model equation was evaluated using multiple correlation coefficients (R^2), R^2-adjusted and predicted residual error sum of squares (PRESS). The optimal combination of input variables for obtaining NPs with desired characteristics (smaller particle size and high EE),

Table 1. Coded levels and ranges of input variables for a 3-level 3-factor BBED to optimize ACE-I-ALG-CS NPs.

Input variable	Level of variables		
	Low (-1)	Medium (0)	High (+1)
Chitosan concentration (%w/v)	0.20	0.35	0.50
Homogenization speed (rpm)	5000	6500	8000
Homogenization time (min)	20	25	30

was determined from predicted values by the model and verified through experimental replication, to ensure the precision of the model's predictions.

2.7. In vivo antihypertensive effect

The *in vivo* antihypertensive efficacy of the ACE-I-ALG-CS NPs was assessed in SHRs. Twenty four rats were divided into four groups, each containing six rats, and were acclimatized for one week under controlled conditions. They had free access to water and standard laboratory diet. The rats in each group received a single dose via oral gavage. Group I received blank ALG-CS NPs (2 mg/kg), Group II received unencapsulated peptide (2 mg/kg), Group III received captopril (2 mg/kg), and Group IV received ACE-I-ALG-CS NPs (2 mg/kg). The NPs were dissolved in normal saline and 0.1 N HCl, and adjusted the volume for each dose before administration, based on the rats' body weight. The rats were placed on a heated platform at 35 °C and the blood pressure was measured using a non-invasive tail cuff instrument (Kent Scientific Corporation, Toorington, CT, USA) at 0 h before administration and at 2, 4, 6, 8, and 24 h post-administration.

2.8. Statistical analysis

Statistical analyses were carried out in triplicate, and data were expressed as mean ± standard deviation. Significant differences between means of SBP of SHRs were determined using t-test. ANOVA followed by Fisher post hoc test was also carried-out to identify significant differences at $p < 0.05$. All data analyses were performed using Minitab statistical software version 16.0.

3. Results and discussion

Prior to encapsulation, the peptide (Ala-Leu-Gly-Pro-Gln-Phe-Tyr) was analyzed for *in vitro* ACE-inhibitory effect and its IC_{50} was determined. Then, the peptide was loaded into ALG-CS NPs through ionic gelation and polyelectrolyte complexation to synthesize the ACE-I-ALG-CS NPs. The NPs were optimized for small particle size and high EE using BBED. Subsequently, the NPs were evaluated for morphology, *in vivo* systolic blood pressure (SBP)-lowering efficacy, and for a 12-weeks physico-chemical storage stability at three different temperatures (2 °C, 7 °C and 12 °C).

3.1. BBED, graphical optimization and model validation for the preparation of ACE-I-ALG-CS NPs

The ACE-I-ALG-CS NPs were prepared by ionic gelation and polyelectrolyte complexation, employing various conditions determined by BBED. This design aimed to encapsulate the low molecular weight ACE-inhibitory peptide, Ala-Leu-Gly-Pro-Gln-Phe-Tyr (Table 2). The BBED comprised 15 experimental runs, with 12 factorial points and 3 center point repetitions per block to estimate the sum of squares for pure error. Each experiment was conducted in triplicate, and the significance of the model and its terms were assessed by ANOVA at $p < 0.05$. Experiments were carried out under the

Table 2. Box Behnken experimental design, predicted and response values due to the two input variables under different formulation conditions.

Run order	Input variables			Output variables			
	X_1	X_2	X_3	Y_1		Y_2	
				Predicted	Experimental	Predicted	Experimental
1	0.35	8000	20	238.08	242.81	54.76	54.82
2	0.50	5000	25	217.11	223.50	55.64	55.70
3	0.35	6500	25	269.28	273.11	71.22	71.10
4	0.20	8000	25	260.30	253.91	70.26	70.20
5	0.35	5000	20	308.04	292.73	55.74	55.52
6	0.50	8000	25	237.51	223.86	55.56	55.34
7	0.35	5000	30	225.63	220.90	70.71	70.65
8	0.35	8000	30	238.47	253.77	71.25	71.47
9	0.20	5000	25	337.82	351.47	70.62	70.84
10	0.50	6500	20	246.09	255.00	56.21	56.36
11	0.50	6500	30	197.70	196.04	72.90	72.90
12	0.35	6500	25	269.28	261.61	71.22	71.28
13	0.35	6500	25	269.28	273.11	71.22	71.29
14	0.20	6500	30	276.83	267.92	86.79	86.63
15	0.20	6500	20	310.46	312.12	72.00	72.00

X_1: Chitosan concentration; X_2: Homogenization speed (rpm); X_3: Homogenization time (min); Y_1: Particle size (nm); Y_2: Encapsulation efficiency (%).

predicted encapsulation conditions to statistically validate the predicted responses (Table 2). The three input variables, including chitosan concentration (X_1), homogenization speed (X_2), and homogenization time (X_3), were analyzed for their main, quadratic, and interaction effects on the particle size (Y_1) and EE (Y_2), as the two response variables (Table 2).

Graphical optimization was conducted to identify the optimal combination of input variables for producing ACE-I-ALG-CS NPs with small particle size and higher EE using response optimizer (Fig. 1). The response optimizer is a crucial component of optimization through RSM, predicting the most favorable levels of input variables or encapsulation conditions. These factors collectively contribute to achieving optimal output, such as small particle size and high EE, based on statistically fitted models.

The optimal predicted levels of the three input variables, designated as X_1 (0.420), X_2 (6000 rpm), and X_3 (30 min), were used to formulate the optimized ACE-I-ALG-CS NPs. These conditions were expected to result in a particle size (Y_1) of 210.81 nm and an EE (Y_2) of 75.30%. Comparison between predicted and experimental values showed no statistically significant differences, with experimental values of 212.60 nm for Y_1 and 74.48% for Y_2. These optimized conditions achieved a combined desirability score of 1.0, with individual desirability scores of 1.0 each for Y_1 and Y_2.

ANOVA results for the quadratic polynomial models are provided in Table 3. Terms involving input variables with non-significant effects ($P > 0.05$) were omitted from the models. Subsequently, linear, quadratic, and interaction model fittings were applied to the two response factors to statistically validate the polynomial equations.

The derived polynomial equations expressing the effect of the input variables on particle size (Y_1) and encapsulation efficiency (Y_2) are as follows:

For Y_1:

$$Y_1 = 270.56 - 36.29X_1 - 13.10X_2 - 22.10X_3 - 6.3X_2^2 - 11.71X_3^2 + 24.48X_1X_2 - 3.69X_1X_3 + 20.70X_2X_3 \quad (4)$$

For Y_2:

$$Y_2 = 71.22 - 7.42X_1 - 0.11X_2 + 7.87X_3 + 0.33X_1^2 - 8.53X_2^2 + 0.42X_3^2 + 0.48X_1X_3 + 0.38X_2X_3 \quad (5)$$

The model fitness and the effects of input variables on outcome values were assessed by significance of β-coefficients through ANOVA. As presented in Table 3, analysis of the fitted quadratic polynomial models showed that, certain factors and their interactions significantly influenced the modeling for particle size and EE. In the particle size model, factors X_1, X_2, X_3, X_{22}, X_{33}, and interactions X_1X_2, X_1X_3, and X_2X_3 were significant. For EE,

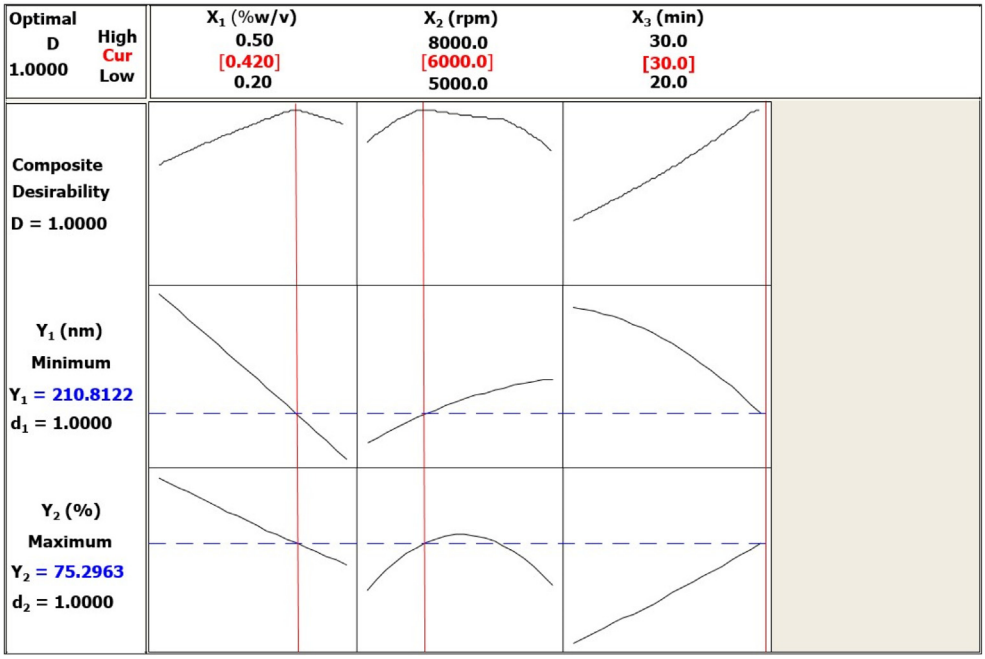

Fig. 1. Response optimization for the preparation of ACE-I-ALG-CS NPs. Individual and composite desirabilities (d_1, d_2 and D) for the predicted responses; Y_1: Particle size, Y_2: Encapsulation efficiency, X_1: Chitosan concentration, X_2: Homogenization speed and X_3: Homogenization time.

Table 3. Analysis of variance of the fitted quadratic models for the mean particle size (Y_1) and Encapsulation efficiency (Y_2).

Source	SS		DF		MS		F		P		Remarks
	Y_1	Y_2	Y_1	Y_2	Y_1	Y_2	Y_1	Y_2	Y_1	Y_2	
Model									0.000	0.000	Significant
Linear											
X_1	10535.70	440.60	1	1	10535.70	440.60	1947.02	7987.91	0.000	0.000	
X_2	1372.40	0.10	1	1	1372.40	0.097	253.61	1.75	0.000	0.243	
X_3	3908.20	495.34	1	1	3908.20	495.34	722.24	8980.29	0.000	0.000	
Quadratic											
X_1X_1	4.30	0.40	1	1	4.30	0.395	0.79	7.16	0.414	0.044	
X_2X_2	146.20	268.68	1	1	146.20	268.682	27.03	4871.10	0.003	0.000	
X_3X_3	506.20	0.66	1	1	506.20	0.658	93.54	11.93	0.000	0.018	
Interaction											
X_1X_2	2397.10	0.02	1	1	2397.10	0.020	442.99	0.36	0.000	0.577	
X_1X_3	54.50	0.91	1	1	54.50	0.912	10.07	16.53	0.025	0.010	
X_2X_3	1714.00	0.58	1	1	1714.00	0.578	316.74	10.47	0.000	0.023	
Total	20638.60	1207.29	9	9	20638.60	1207.282	3814.03	21887.50			
Residual Error	27.1	0.28	5	5	5.40	0.055					
Pure Error	9.80	0.02	2	2	4.90	0.011					
Lack of Fit	17.30	0.25	3	3	5.80	0.084	1.18	7.37	0.490	0.122	Non-significant

R_1 (R^2 = 99.87%, R^2 − predicted = 98.55, R^2 − adjusted = 99.63%, S.D = 2.326, PRESS = 298.431
R_2 (R^2 = 99.98%, R^2 − predicted = 99.66%, R^2 − adjusted = 99.94%, S.D = 0.235, PRESS = 4.098

variables X_1, X_3, X_{11} X_{22}, X_{33}, and interaction terms X_1X_3 and X_2X_3 were statistically significant ($p < 0.05$).

Equations (4) and (5) indicated that higher levels of factor X_1 led to decreases in both particle size (Y_1) and EE (Y_2) due to increased chitosan concentration and low peptide load. Conversely, higher levels of factor X_2 increased Y_1 and decreased Y_2 when peptide load was high at a low chitosan/peptide mass ratio. Factor X_3 had opposite effects on Y_1 and Y_2, with an increase resulting in reduced particle size and increased EE.

The observed decrease in particle size could be attributed to the formation of more electrostatic interactions at high chitosan concentration and low peptide load, stabilizing the NPs and preventing peptide leakage. The decrease in EE might be due to the limited amount of peptide incorporated into the nanocarrier particles at low peptide load and the rupture of coating materials releasing the entrapped peptide. Conversely, higher EE could result from a higher peptide load [25]. The increase in particle size might be related to low chitosan concentration, where available polycationic surfaces of chitosan were inadequate to ionically gelate their counter ions on alginate, to strength their interaction and minimize particle size [20].

The involvement of quadratic and interaction terms in the regression equation suggests nonlinear relationships between input variables and responses. Three-dimensional response surface plots illustrating how the responses were related to input variables as well as interaction effects of pairs of factors (X_1X_2, X_1X_3, and X_2X_3) on particle size (Y_1) and encapsulation efficiency (Y_2) are depicted in Fig. 2.

The Fig. 2(a) and (d) illustrate the combined effects of homogenization speed (X_2) and homogenization time (X_3) on Y_1 and Y_2 with a fixed chitosan concentration (X_1) of 0.35% w/v. In this scenario, X_2 demonstrated a synergistic effect on Y_1 and an antagonistic effect on Y_2. Factor X_3 showed a synergistic effect that was only significant for Y_2. The interaction between X_2 and X_3 resulted in a significant positive effect on both Y_1 and Y_2.

The Fig. 2(b) and (e) depict the combined effect of X_1 and X_3 on Y_1 and Y_2 with a constant X_2 value of 6500 rpm. Here, X_1 showed a synergistic effect on both Y_1 and Y_2, while X_3 displayed a synergistic effect that was significant only for Y_2. The interaction between X_1 and X_3 resulted in a significant positive effect on both Y_1 and Y_2.

The Fig. 2(c) and (f) illustrate the combined effect of X_1 and X_2 on Y_1 and Y_2 with X_3 held constant at 25 min. In this case, X_1 exhibited a significant synergistic effect on both Y_1 and Y_2, while X_2 showed a synergistic effect on Y_1 and an antagonistic effect on Y_2, both significant at $p < 0.05$. The interaction between X_1 and X_2 revealed a significant synergistic effect on Y_1 and an antagonistic effect on Y_2.

The fitness of the models and the significant effects of input variables on outcomes were assessed using the coefficient of determination (R-squared) values and ANOVA. The full quadratic models showed the highest R-squared (R^2) values of 99.87%

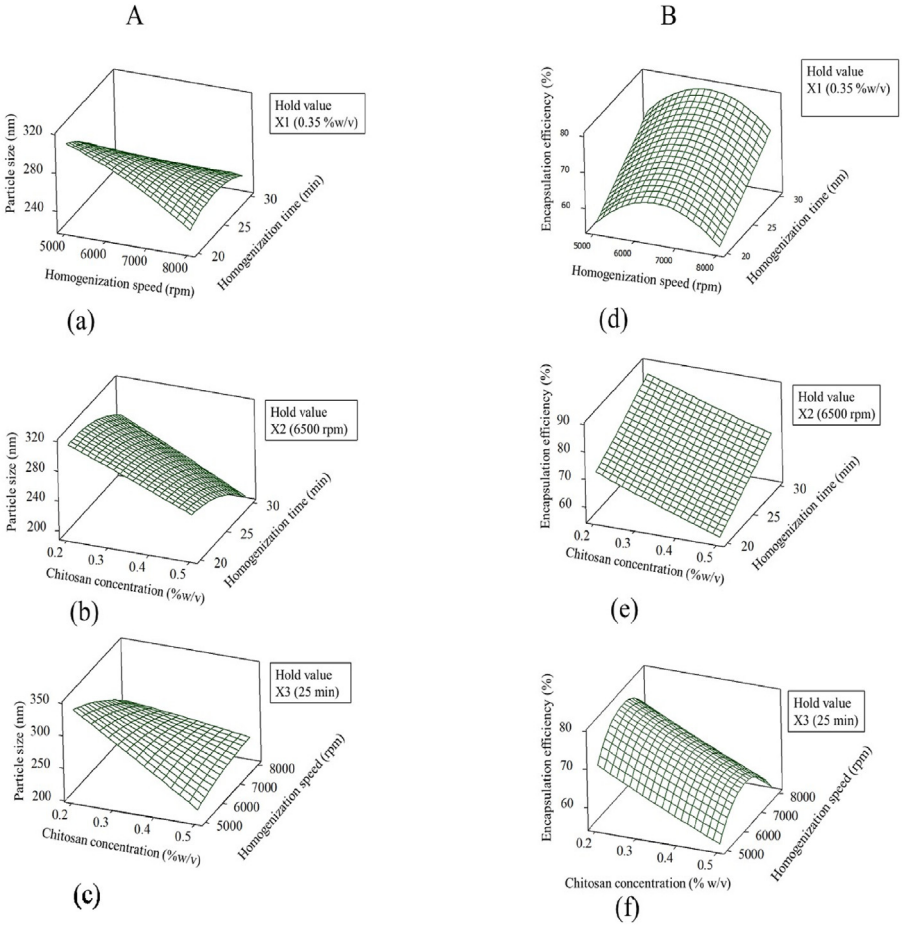

Fig. 2. Three-dimensional response surface plots for the effect of input variables on; (A). Particle size: (a) homogenization speed (X_2) and Homogenization time (X_3); (b) Chitosan concentration (X_1) and Homogenization time (X_3); (c) Chitosan concentration (X_1) and Homogenization speed (X_2), (B). Encapsulation efficiency (%): (d) Homogenization speed (X_2) and Homogenization time (X_3); (e) Chitosan concentration (X_1) and Homogenization time (X_2); (f) Chitosan concentration (X_1) and Homogenization speed (X_2).

and 99.98% as well as PRESS values of 298.431 and 4.098 for Y_1 and Y_2, respectively, and were selected as the best fit models (Table 3).

High F-values of 422.91 and 2444.70 for Y_1 and Y_2 models indicated their significant influence on Y_1 and Y_2 responses, supported by F-value probabilities of $p < 0.05$ for both Y_1 and Y_2. The lack-of-fit values of 0.490 and 0.122 for Y_1 and Y_2 were insignificant, indicating a strong correlation between input and output variables for each model.

The non-significant difference ($p < 0.05$) in the values of R^2-adjusted and R^2-predicted for both Y_1 and Y_2 confirmed the validity and statistical significance of the equations in optimizing ACE-I-ALG-CS NPs. The reliability and validity of the final models were further confirmed by comparing actual response values with fitted values derived from the response regression equation [26].

However, the Y_1 and Y_2 models for the particle size and the EE revealed differences in their predictive accuracy based on PRESS. The Y_1 with a PRESS value of 298.431, exhibited higher level of deviation from actual values, indicating lower predictive accuracy and reliability. In contrast, the Y_2 with a PRESS value of 4.098, showed a minimal deviation with higher predictive accuracy and reliability. Therefore, Y_2 can be inferred to be more effective and reproducible compared to Y_1. In a related study, the selection of quadratic model for the phytofabricated chitosan nanoparticles, was conducted using BBED based on higher values of R^2, adjusted-R^2, predicted-R^2, lower values of standard deviation, probability (P) and the PRESS [27].

3.2. Physicochemical stability

The optimized ACE-I-ALG-CS NPs were stored at 2 °C, 7 °C and 12 °C, and assessed for physicochemical stability by monitoring changes in their particle size, pdi, ζ and EE, once weekly for 12 weeks (Fig. 3).

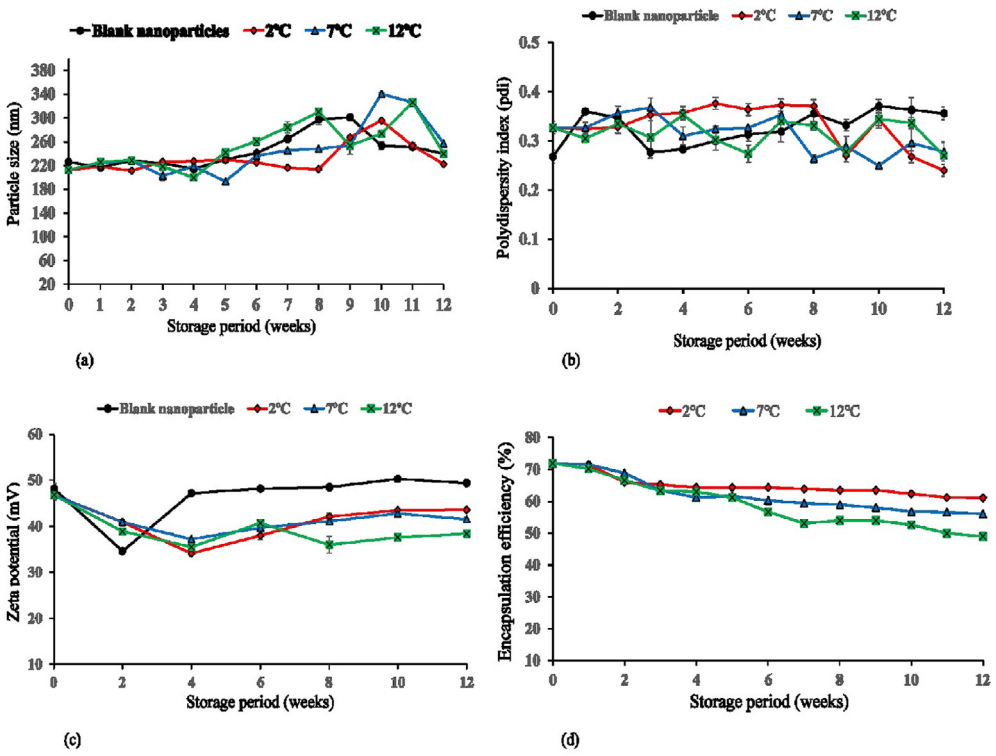

Fig. 3. Changes in the physicochemical characteristics of the optimized ACE-I-ALG-CS NPs loaded with low molecular weight ACE-inhibitory peptide (Ala-Leu-Gly-Pro-Gln-Phe-Tyr) during a 12-week storage period at temperatures of 4 °C, 7 °C, and 12 °C: (a) Changes in particle size (b) Changes in polydispersity index (c) Changes in zeta potential, and (d) Changes in encapsulation efficiency.

Initial measurements before storage showed particle size of 212.60 nm, pdi of 0.327, ζ of +46.8 mV, and EE of 74.48%, respectively. After 12 weeks of storage, changes were observed in these indices with the new values of 222.2 nm, 257.30 nm and 239.90 nm for particle size; 0.240, 0.278 and 0.270 for pdi; +49.40 mV, +43.60 mV and +38.40 mV for ζ as well as 61.03%, 56.05% and 49.01% for EE at 2 °C, 7 °C and 12 °C, respectively (Fig. 3). Significant changes in particle size were observed by the 5th week at 7 °C and 12 °C, and by the 9th week at 2 °C (Fig. 3a), likely due to nanoparticle swelling.

Similarly, significant changes in pdi were observed during the 6th, 8th and 9th weeks at 12 °C, 7 °C, and 2 °C, respectively (Fig. 3b), but pdi values remained below 0.5, indicating minimal aggregation and high dispersion of NPs. Despite variations in these indices, the stability of ACE-I-ALG-CS NPs remained substantial throughout storage, indicating the effectiveness of alginate and chitosan as coating materials for nanocarrier systems, facilitating successful delivery of encapsulated peptides [21].

The ζ reflecting surface charge, remained high and positively charged, indicating strong electrostatic repulsion among nanoparticles, thereby preventing aggregation and enhancing colloidal stability [20]. However, significant changes in ζ were observed by the 4th week of storage at all temperatures, with sustained stability observed at 2 °C and 7 °C after 12th week (Fig. 3c).

The results of the EE, indicating the degree of peptide integration into the ACE-I-ALG-CS NPs are presented in Fig. 3d. Achieving high EE values for peptides can enhance their bioavailability and efficacy upon oral administration. A notable decrease in EE ($p < 0.05$) occurred for NPs stored at 12 °C and 7 °C by the 6th and 8th week, respectively, likely due to peptide release stemming from excessive loading, NPs swelling and degradation [25]. Moreover, the decrease in EE was accompanied by mild aggregation and rupture of the NPs, leading to the leakage of encapsulated peptides. In addition, the heterogeneous nature of peptides often affect their behavior and EE within nanocarrier systems. Consequently, the selection of an appropriate encapsulation technique and polymer concentrations, is crucial to achieve high EE and maintain the stability and bioactivity of loaded peptides [28].

Thus, in the present study, the optimum concentration of chitosan (0.420%w/v) was selected to fabricate ACE-I-ALG-CS NPs with sustained physicochemical stability (small particle size, low pdi, high

ζ and EE). These properties are necessary to facilitate mucoadhesion and absorption of the nanocarriers for controlled release of the encapsulated peptide, thereby enhancing its bioavailability [28,29]. Moreover, the selected concentration was to maintain the solubility and compatibility of the polymer with other formulation components, thereby preventing any adverse interactions. In addition, the concentration of chitosan was selected by considering its molecular weight and deacetylation for optimal ACE-I-ALG-CS NPs size. The net effect for the selection was to ensure higher stability, effective oral delivery and enhanced efficacy of the peptide for *in vivo* hypertension management [28,30].

In a related study, Danish et al. [31] examined the storage stability of chitosan NPs containing a fish-derived ACE-inhibitory tripeptide (LPK), and observed changes in particle size, pdi, ζ, and EE. Similarly, Azari et al. [32] reported improved physicochemical stability of phycocyanin-loaded nanoliposomes coated with chitosan at an optimal concentration, with increased EE following storage. Additionally, Cao et al. [33] demonstrated sustained EE enhancement due to chitosan coating of nanoliposomes loaded with a walnut-derived ACE-inhibitory peptide. Moreover, Reyhani Poul and Yeganeh [34] reported increased EE and colloidal stability due to chitosan coating of shrimp waste-derived peptide-loaded nanoliposomes at different concentrations.

3.3. Transmission electron microscopy (TEM)

The morphology of the nanocarriers was studied using TEM imaging which provides highly powerful magnification suitable for the examination of nanocarriers. As shown in Fig. 4, the TEM images for the ACE-I-ALG-CS NPs are in form of discrete spherical particles (Fig. 4). This observation is further supported by the low pdi values (<0.5) of the nanocarriers, indicating high dispersion of the NPs suspension (Fig. 3b).

3.4. In vitro ACE-inhibitory activity and in vivo antihypertensive efficacy

3.4.1. In vitro ACE-inhibitory activity

The low molecular weight peptide (Ala-Leu-Gly-Pro-Gln-Phe-Tyr, 794 Da) consisted of neutral, aliphatic, branched chain, non-polar and aromatic amino acids residues. An *in vitro* assay, demonstrated a high ACE-inhibitory activity of 94.43 ± 2.05% and an IC_{50} of 0.012 ± 0.001 mM for the peptide. The high ACE-inhibitory activity was related to the presence of aromatic Phe and Tyr at C-terminal, aliphatic Ala and branched chain Leu at the N-terminal as well as proline at 4th position from the C-terminal [1].

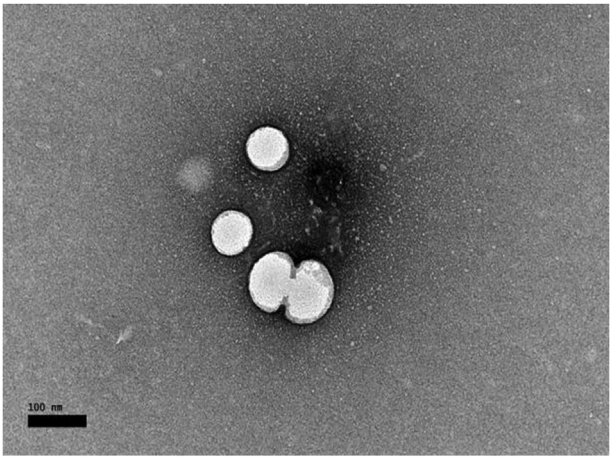

Fig. 4. Transmission electron microscopy of the ACE-I-ALG-CS NPs prepared by ionic gelation and polyelectrolyte complexation.

3.4.2. In vivo antihypertensive efficacy

The antihypertensive efficacy of various treatments (ALG-CS NPs, unencapsulated peptide, captopril and ACE-I-ALG-CS NPs) was assessed through their 24 h SBP-lowering effect on SHRs (Fig. 5). The negative control group (ALG-CS NPs) exhibited no significant change in SBP within the 24 h post-administration (Fig. 5). A single oral dose of 2 mg/kg for both unencapsulated peptide, captopril and ACE-I-ALG-CS NPs resulted in significant ($p < 0.05$) reduction in the mean SBP of SHRs within the 24 h post-oral administration compared to the negative control.

Similar to its strong *in vitro* ACE-inhibitory activity, the peptide exhibited high *in vivo* antihypertensive effect on SHRs. Notably, a significant antihypertensive effect was observed within 24 h of Ala-Leu-Gly-Pro-Gln-Phe-Tyr administration, with peak activity observed at the 8th h post-administration. The SBP-lowering effect of the peptide was found to be similar to that of captopril. Since captopril is a chemically designed and commercially available drug, this suggests the potential of Ala-Leu-Gly-Pro-Gln-Phe-Tyr in the development of novel antihypertensive treatment. However, captopril exerted its peak activity at 6th h post-oral administration. The ACE-I-ALG-CS NPs treated group showed significantly higher ($p < 0.05$) reduction in SBP during the 24 h post oral treatment compared to other groups. The peak activity of the ACE-I-ALG-CS NPs was observed by the 8th h post administration which remained sustained even at the 24th h of post-administration. The peak activity exerted by unencapsulated peptide,

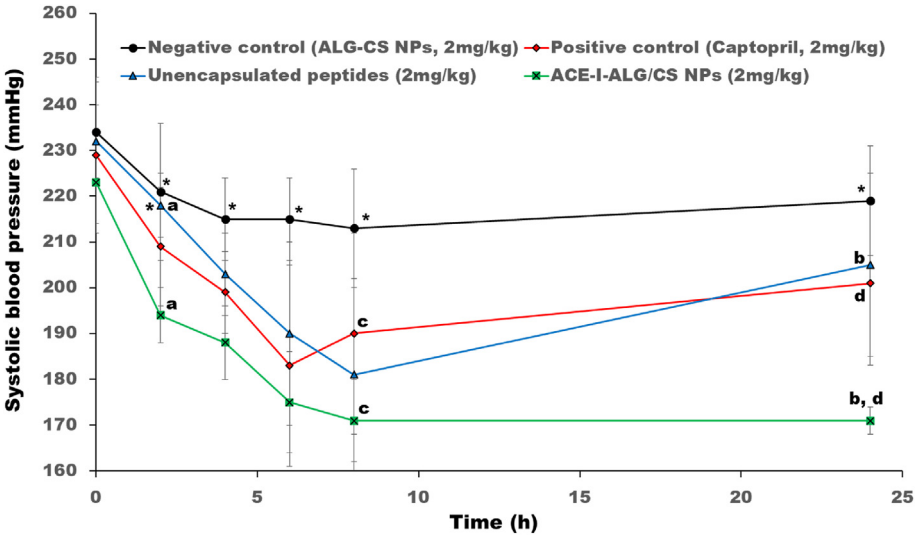

Fig. 5. A 24 h SBP-lowering effect of a single oral dose of ALG-CS NPs, unencapsulated peptide, captopril and ACE-I-ALG-CS NPs on SHRs. Means of SBP with asterisk are not significantly different at $p < 0.05$ compared to each other, at the same hour post administration. Means of SBP sharing a common letter are significantly different at $p < 0.05$ compared to each other, at the same hour post treatment.

captopril and ACE-I-ALG-CS NPs corresponded to 13.16%, 14.88% and 19.72% reduction in the SBP of the SHRs, respectively. The improved antihypertensive efficacy of the ACE-I-ALG-CS NPs, may stem from the enhanced stability, intestinal absorption, and bioavailability of the encapsulated peptide, facilitated by the stabilized physicochemical characteristics of nanocarriers due to the coating polymers [28,30].

The physicochemical characteristics of nanocarriers including particle size, pdi, zeta potential, and EE, have been shown to significantly influence their *in vivo* efficacy [35]. Smaller particle size enhances absorption and bioavailability, while a low pdi ensures homogeneity and stability [36]. Similarly, a high absolute zeta potential value improves colloidal stability and have been reported to promote cellular uptake of nanocarriers [28].

The work of Sorasitthiyanukarn et al. [37] demonstrated improved physicochemical stability, digestibility, bioaccessibility, and cellular uptake of curcumin encapsulated in chitosan/alginate NPs with small particle size, high zeta potential and EE. In another research, quercetin-loaded alginate/chitosan NPs, with small particle sizes and high EE revealed an enhanced protective activity of quercetin against systemic toxicity [38]. Similarly, resveratrol-loaded alginate/chitosan NPs provided sustained release and higher cellular uptake due to its smaller particle size and higher EE [39]. Moreover, high EE has been observed to facilitate sufficient peptide loading and a controlled release profile for peptide [21]. Hence, these properties might have synergistically enhanced the stability, targeted delivery and therapeutic effects, while minimizing off-target effects and optimizing effectiveness and safety of the ACE-I-ALG-CS NPs for sustained blood pressure control in the SHRs. Therefore, the combined application of alginate-chitosan as nanocarriers, enhances the controlled delivery of bioactive compounds in the gastrointestinal tract, thus improving their stability, bioaccessibility, and bioavailability [28].

The alginate-chitosan coating provides protection to encapsulated peptide against enzymatic and hydrolytic degradation in the GIT. However, the higher pH and ionic environment of the small intestines, facilitates gradual breakdown of nanocarriers, leading to a slow and controlled release of the encapsulated peptide [40]. A consistent release of the peptide into bloodstream, could maintain a steady blood pressure level within 24 h of nanocarriers post oral administration. Hence, the observed peak in SBP decrease at 8 h post oral administration, could be due an initial burst of ACE-I-ALG-CS NPs with prolonged release of the peptide at an effective concentrations. This might have been fine-tuned to enhance its therapeutic efficacy and sustained the decrease in blood pressure levels within the 24 h post oral administration [20,25].

Previously, Danish et al. [41] reported a reduction in the SBP of SHRs due to chitosan-zein coating of two food derived tripeptides (IPP and LKP) with prolong SBP-lowering effect within 8 h post oral administration similar to captopril, and was attributed to the enhanced release properties of the NPs.

In addition, Michalowski et al. [42] attributed the sustained blood pressure lowering effect and protection of renal functions of SHRs, to the coating materials including chitosan, for their prepared Captopril-Surface Functionalized Furosemide-Loaded Multi-Wall Lipid-Core Nanocapsules.

The alginate-chitosan nanocarriers exhibits distinct biodistribution pattern following their oral administration in rats [43–45]. At first, the nanocarriers navigates the acidic environment of the stomach while preventing its encapsulated peptides against degradation. In the small intestine, the nanocarriers bypasses the epithelial barrier through paracellular and transcellular transports [30,46,47]. This facilitates the entry of the bioactive peptides into systemic circulation to the target site of action. In this scenario, alginate-chitosan nanocarriers have been used as effective oral delivery systems, to enhance the bioavailability and therapeutic efficacy of peptide on target tissues [13,29]. It has been shown that, once absorbed, the alginate-chitosan nanocarriers are distributed to various organs, including liver, spleen, kidneys, and lungs. This is finally followed by their excretion at a specific clearance rate to protect the body against any adverse effect [48,49].

The clearance rate of the nanocarriers is essentially useful to understand their pharmacokinetics, efficacy, safety and toxicity profile. It enhances the overall performance of nano delivery systems for effective therapeutic payload while minimizing adverse effects [50]. As previously reported, a portion of nanocarriers is absorbed and the encapsulated peptide is released into systemic circulation during the first few hours post-administration [51]. Thus, within the period of post administration, a significant portion of the non-absorbed nanocarriers might be excreted from the body via feces, whereas the absorbed fractions could be processed and eliminated through renal and hepatic pathways [51–53]. In this way, clearance ensures therapeutic efficacy, minimises the risk of long-term accumulation and reduces toxicity and side effects due to nanocarriers. This controlled degradation and clearance makes alginate-chitosan nanocarriers to be safe and effective for oral delivery of bioactive peptides [50,54].

4. Conclusion

In this study, ACE-I-ALG-CS NPs were synthesized as nanocarriers for Ala-Leu-Gly-Pro-Gln-Phe-Tyr and optimized using a three-factor, three-level Box Behnken design. The optimal conditions, including a chitosan concentration of 0.42% w/v, homogenization speed of 6000 rpm, and homogenization time of 30 min, yielded nanocarriers with a small particle size (212.60 nm) and high EE (74.48%). The enhanced *in vivo* antihypertensive efficacy of Ala-Leu-Gly-Pro-Gln-Phe-Tyr was attributed to the ACE-I-ALG-CS NPs, which provided gastrointestinal stability and sustained reduction in SBP of SHRs for up to 24 h post-oral administration, significantly surpassing the effects of captopril and unencapsulated peptide. Furthermore, physicochemical stability assessments over 12 weeks indicated stable nanocomposites with sustained monodispersion, high colloidal stability, and EE at various storage temperatures (4 °C, 7 °C, and 12 °C). Therefore, the ACE-I-ALG-CS NPs prepared via ionic gelation and polyelectrolyte complexation demonstrate capability as successful nanocarriers for improving the physicochemical stability, bioavailability, and *in vivo* efficacy of food-derived peptides, facilitating their incorporation as therapeutic ingredients into functional food formulations.

Thus, the optimized nanocarriers exhibited high physicochemical stability and demonstrated a sustained *in vivo* peptide release with significant SBP reduction in SHRs. However, their application may be limited by challenges related to complexities in optimization, physicochemical stability, *in vivo* variability, bioavailability, absorption, toxicity, and immunogenicity. Hence, the nanocarriers may be enhanced with stimuli-responsive properties for smart, personalized delivery through targeted release. In addition, more extensive *in vivo* studies may be necessary to elucidate their toxicity profiles as well as mode of response to both chemical and physical stimuli, for precise delivery of the encapsulated peptides. Furthermore, it is important to evaluate the expected lifetime of the nanocarriers in human body to ensure they last long enough to fully perform their intended functions with higher stability, safety and efficacy. Finally, regulatory pathways may be required to establish an effective and safe therapeutic application of the nanocarriers for treatment of hypertension.

Author contributions

Conceptualization: Nazamid Saari, Shehu Muhammad Auwal; Data curation: Balqis Muhammad Ghanisma, Shehu Muhammad Auwal; Funding acquisition: Nazamid Saari; Analysis and interpretation of data: Balqis Muhammad Ghanisma, Shehu Muhammad Auwal; Resources: Nazamid Saari, Shehu Muhammad Auwal; Writing of the original draft: Shehu Muhammad Auwal; Review & editing: Nazamid Saari, Shehu Muhammad Auwal.

Conflicts of interest statement

No conflict of interest exists.

Acknowledgements

We acknowledged the financial support from the Ministry of Science, Technology and Innovation, Malaysia under the project No. 02-01-04-SF 2309.

References

[1] Auwal SM, Zainal Abidin N, Zarei M, Tan CP, Saari N. Identification, structure-activity relationship and in silico molecular docking analyses of five novel angiotensin I-converting enzyme (ACE)-inhibitory peptides from stone fish *(Actinopyga lecanora)* hydrolysates. PLoS One 2019;14: e0197644.

[2] Su Y, Chen S, Shen J, Yi Z, Liu S, Cai S, et al. Screening and molecular Mechanisms of novel ACE-inhibitory peptides from *Gracilariopsis lemaneiformis*. Int J Mol Sci 2022;23: 14850.

[3] Xie D, Shen Y, Su E, Du L, Xie J, Wei D. The effects of angiotensin I converting enzyme inhibitory peptide VGINYW and the hydrolysate of α-lactalbumin on blood pressure, oxidative stress and gut microbiota of spontaneously hypertensive rats. Food Funct 2022;13:2743−55.

[4] Aguilar-Toalá JE, Quintanar-Guerrero D, Liceaga AM, Zambrano-Zaragoza ML. Encapsulation of bioactive peptides: a strategy to improve the stability, protect the nutraceutical bioactivity and support their food applications. RSC Adv 2022;12:64496458.

[5] Patil PJ, Usman M, Zhang C, Mehmood A, Zhou M, Teng C, et al. An updated review on food-derived bioactive peptides: focus on the regulatory requirements, safety, and bioavailability. CRFSFS 2022;21:1732−76.

[6] Bashir S, Fitaihi R, Abdelhakim HE. Advances in formulation and manufacturing strategies for the delivery of therapeutic proteins and peptides in orally disintegrating dosage forms. Eur J Pharm Sci 2023;182:106374.

[7] Verma S, Goand UK, Husain A, Katekar RA, Garg R, Gayen JR. Challenges of peptide and protein drug delivery by oral route: current strategies to improve the bioavailability. Drug Dev Res 2021;82:927−44.

[8] Pei J, Gao X, Pan D, Hua Y, He J, Liu Z, et al. Advances in the stability challenges of bioactive peptides and improvement strategies. CRFS 2022;5:2162−70.

[9] Zhu Y, Lao F, Pan X, Wu J. Food protein-derived antioxidant peptides: molecular mechanism, stability and bioavailability. Biomol 2022;12:1622.

[10] Iwaniak A, Hrynkiewicz M, Bucholska J, Minkiewicz P, Darewicz M. Understanding the nature of bitter-taste di-and tripeptides derived from food proteins based on chemometric analysis. J Food Biochem 2019;43:e12500.

[11] Hosseini SF, Ramezanzade L, McClements DJ. Recent advances in nanoencapsulation of hydrophobic marine bioactives: bioavailability, safety, and sensory attributes of nano-fortified functional foods. Trends Food Sci Technol 2021;109:322339.

[12] Han C, Fang L, Song S, Min W. Polysaccharides-based delivery system for efficient encapsulation and controlled release of food-derived active peptides. Carbohydr Polym 2022;291:119580.

[13] Niculescu AG, Grumezescu AM. Applications of chitosan-alginate-based nanoparticles—an up-to-date review. Nanomaterials 2022;12:186.

[14] Hua Y, Wei Z, Xue C. Chitosan and its composites-based delivery systems: advances and applications in food science and nutrition sector. Crit Rev Food Sci Nutr 2023;63: 4579−98.

[15] Bajpai VK, Kamle M, Shukla S, Mahato DK, Chandra P, Hwang SK, et al. Prospects of using nanotechnology for food preservation, safety, and security. J Food Drug Anal 2018;26: 1201−14.

[16] He X, Deng H, Hwang HM. The current application of nanotechnology in food and agriculture. J Food Drug Anal 2019;27:1−21.

[17] Sorasitthiyanukarn FN, Muangnoi C, Rojsitthisak P, Rojsitthisak P. Chitosan-alginate nanoparticles as effective oral carriers to improve the stability, bioavailability, and cytotoxicity of curcumin diethyl disuccinate. Carbohydr Polym 2021;256:117426.

[18] Li D, Wei Z, Xue C. Alginate-based delivery systems for food bioactive ingredients: an overview of recent advances and future trends. CRFSFS 2021;20:5345−69.

[19] Loquercio A, Castell-Perez E, Gomes C, Moreira RG. Preparation of chitosan-alginate nanoparticles for trans-cinnamaldehyde entrapment. J Food Sci 2015;80:N2305−15.

[20] Auwal SM, Zarei M, Tan CP, Basri M, Saari N. Enhanced physicochemical stability and efficacy of angiotensin I-converting enzyme (ACE)-inhibitory biopeptides by chitosan nanoparticles optimized using Box-Behnken design. Sci Rep 2018;8:10411.

[21] Yuan H, Guo C, Liu L, Zhao L, Zhang Y, Yin T, et al. Progress and prospects of polysaccharide-based nanocarriers for oral delivery of proteins/peptides. Carbohydr Polym 2023;312: 120838.

[22] Auwal SM, Zarei M, Tan CP, Basri M, Saari N. Improved *in vivo* efficacy of anti-hypertensive biopeptides encapsulated in chitosan nanoparticles fabricated by ionotropic gelation on spontaneously hypertensive rats. Nanomaterials 2017;7: 421.

[23] Tang W, Wang J, Hou H, Li Y, Wang J, Fu J, et al. Application of chitosan and its derivatives in medical materials. Int J Biol Macromol 2023:124398.

[24] Jimsheena VK, Gowda LR. Colorimetric, high-throughput assay for screening angiotensin I-converting enzyme inhibitors. Anal Chem 2009;81:9388−94.

[25] Auwal SM, Ghanisma SBM, Saari N. Improved systolic blood pressure (SBP)-lowering effect of stone fish-derived angiotensin-I converting enzyme (ACE)-inhibitory peptide entrapped in chitosan-coated alginate nanocomposites. Food Biosci 2024;60:104349.

[26] Auwal SM, Zarei M, Abdul-Hamid A, Saari N. Optimization of bromelain-aided production of angiotensin I-converting enzyme inhibitory hydrolysates from stone fish using response surface methodology. Mar Drugs 2017;15:104.

[27] El-Naggar NE, Saber WI, Zweil AM, Bashir SI. An innovative green synthesis approach of chitosan nanoparticles and their inhibitory activity against phytopathogenic Botrytis cinerea on strawberry leaves. Sci Rep 2022;12:3515.

[28] Karim A, Rehman A, Feng J, Noreen A, Assadpour E, Kharazmi MS, et al. Alginate-based nanocarriers for the delivery and controlled-release of bioactive compounds. Adv Colloid Interface Sci 2022;307:102744.

[29] Wang Q, Dong X, Castañeda-Reyes ED, Wu Y, Zhang S, Wu Z, et al. Chitosan and sodium alginate nanocarrier system: controlling the release of rapeseed-derived peptides and improving their therapeutic efficiency of anti-diabetes. Int J Biol Macromol 2024;265:130713.

[30] Peng S, Song H, Chen Y, Li S, Guan X. Oral Delivery of food-derived bioactive peptides: challenges and strategies. Food Rev Int 2023;39:5297−325.

[31] Danish MK, Vozza G, Byrne HJ, Frias JM, Ryan SM. Formulation, characterization and stability assessment of a food-derived tripeptide, leucine-lysine-proline loaded chitosan nanoparticles. J Food Sci 2017;82:2094−104.

[32] Azari A, Ghaboos SHH, Moghadam VE, Jafari SM. Influence of chitosan coating on the physicochemical and antioxidant properties of phycocyanin-loaded nanoliposomes. Algal Res 2023;72:103120.

[33] Cao S, Hao J, Wang Y, Zhou X, Wang F. Chitosan-coated nanoliposomes for the enhanced stability of walnut

angiotensin-converting enzyme (ACE) inhibitory peptide. J Food Sci 2023;88:2130−40.
[34] Reyhani Poul S, Yeganeh S. Physicochemical and antioxidant properties of chitosan-coated nanoliposome loaded with bioactive peptides produced from shrimp wastes hydrolysis. Iran J Fish Sci 2022;21:987−1003.
[35] Zhao Z, Ukidve A, Krishnan V, Mitragotri S. Effect of physicochemical and surface properties on in vivo fate of drug nanocarriers. Adv Drug Deliv Rev 2019;143:3−21.
[36] Mi Y, Chen Y, Li Q, Tan W, Guo Z. pH sensitive adriamycin-incorporated nanoparticles self-assembled from amphiphilic chitosan derivatives with enhanced antioxidant and antitumor activities. Carbohydr Polym Tech Appl 2024;7:100475.
[37] Sorasitthiyanukarn FN, Bhuket PRN, Muangnoi C, Rojsitthisak P, Rojsitthisak P. Chitosan/alginate nanoparticles as a promising carrier of novel curcumin diethyl diglutarate. Int J Biol Macromol 2019;131:1125−36.
[38] Nalini T, Basha SK, Sadiq AMM, Kumari VS, Kaviyarasu K. Development and characterization of alginate/chitosan nanoparticulate system for hydrophobic drug encapsulation. J Drug Deliv Sci Technol 2019;52:65−72.
[39] Min JB, Kim ES, Lee JS, Lee HG. Preparation, characterization, and cellular uptake of resveratrol-loaded trimethyl chitosan nanoparticles. Food Sci Biotechnol 2018;27:441−50.
[40] Singh J, Nayak P. pH-responsive polymers for drug delivery: trends and opportunities. J Polym Sci 2023;61:2828−50.
[41] Danish MK, Gleeson JP, Brayden DJ, Byrne HJ, Frías JM, Ryan SM. Formulation, characterisation and evaluation of the antihypertensive peptides, isoleucine-proline-proline and leucine-lysine-proline in chitosan nanoparticles coated with zein for oral drug delivery. Int J Mol Sci 2022;23:11160.
[42] Michalowski CB, Arbo MD, Altknecht L, Anciuti AN, Abreu ASG, Alencar LMR, et al. Oral treatment of spontaneously hypertensive rats with captopril-surface functionalized furosemide-loaded multi-wall lipid-core nanocapsules. Pharmaceutics 2020;12:80.
[43] Sonin D, Pochkaeva E, Zhuravskii S, Postnov V, Korolev D, Vasina L, et al. Biological safety and biodistribution of chitosan nanoparticles. Nanomaterials 2020;10:810.
[44] Lakkakula J, Roy A, Krishnamoorthy K, Alghamdi S, Almehmadi M, Gujarathi P, et al. Alginate-based nanosystems for therapeutic applications. J Nanomater 2022:6182815.
[45] Li J, Wen Q, Dai J, Wang B, Lu Y, Wu Z, et al. An oral bioactive chitosan-decorated doxorubicin nanoparticles/bacteria bioconjugates enhance chemotherapy efficacy in an in-situ breast cancer model. Int J Biol Macromol 2024;267:131428.
[46] Alai MS, Lin WJ, Pingale SS. Application of polymeric nanoparticles and micelles in insulin oral delivery. J Food Drug Anal 2015;23:351−8.
[47] Mehrotra S, Bg PK, Nayak PG, Joseph A, Manikkath J. Recent progress in the oral delivery of therapeutic peptides and proteins: overview of pharmaceutical strategies to overcome absorption hurdles. Adv Pharm Bull 2024;14:11.
[48] Kean T, Thanou M. Biodegradation, biodistribution and toxicity of chitosan. Adv Drug Deliv Rev 2010;62:3−11.
[49] Haripriyaa M, Suthindhiran K. Pharmacokinetics of nanoparticles: current knowledge, future directions and its implications in drug delivery. Futur J Pharm Sci 2023;9:113.
[50] Cabral H, Li J, Miyata K, Kataoka K. Controlling the biodistribution and clearance of nanomedicines. Nat Rev Bioeng 2024;2:214−32.
[51] Griffin BT, Guo J, Presas E, Donovan MD, Alonso MJ, O'Driscoll CM, et al. Pharmacokinetic, pharmacodynamic and biodistribution following oral administration of nanocarriers containing peptide and protein drugs. Adv Drug Deliv Rev 2016;106:367−80.
[52] Chehelgerdi M, Chehelgerdi M, Allela OQB, Pecho RDC, Jayasankar N, Rao DP, et al. Progressing nanotechnology to improve targeted cancer treatment: overcoming hurdles in its clinical implementation. Mol Cancer 2023;22:169.
[53] Kuperkar K, Atanase LI, Bahadur A, Crivei IC, Bahadur P. Degradable polymeric bio (nano) materials and their biomedical applications: a comprehensive overview and recent updates. Polymers 2024;16:206.
[54] Guarino V, Caputo T, Altobelli R, Ambrosio L. Degradation properties and metabolic activity of alginate and chitosan polyelectrolytes for drug delivery and tissue engineering applications. AIMS Mater Sci 2015;2:497−502.